A Human-Robot Collaboration Framework for Improving Ergonomics During Dexterous Operation of Power Tools

Wansoo Kim[a,1,*], Luka Peternel[b,1], Marta Lorenzini[a,c], Jan Babič[d], and Arash Ajoudani[a]

[a] *HRI² Lab, Department of Advanced Robotics, Istituto Italiano di Tecnologia, Genoa, Italy*
[b] *Department of Cognitive Robotics, Delft University of Technology, Delft, The Netherlands*
[c] *Department of Electronics, Information and Bioengineering, Politecnico di Milano, Milano, Italy*
[d] *Department of Automation, Biocybernetics and Robotics, Jožef Stefan Institute, Ljubljana, Slovenia*

Abstract

In this work, we present a novel control approach to human-robot collaboration that takes into account ergonomic aspects of the human co-worker during power tool operations. The method is primarily based on estimating and reducing the overloading torques in the human joints that are induced by the manipulated external load. The human overloading joint torques are estimated and monitored using a whole-body dynamic state model. The appropriate robot motion that brings the human into the suitable ergonomic working configuration is obtained by an optimisation method that minimises the overloading joint torques. The proposed optimisation process includes several constraints, such as the human arm muscular manipulability and safety of the collaborative task, to achieve a task-relevant optimised configuration. We validated the proposed method by a user study that involved a human-robot collaboration task, where the subjects operated a polishing machine on a part that was brought to them by the collaborative robot. A statistical analysis of ten subjects as an experimental evaluation of the proposed control framework is provided to demonstrate the potential of the proposed control framework in enabling ergonomic and task-optimised human-robot collaboration.

Keywords: Human-Robot Interaction, Ergonomics, Human performance modelling, Industrial/organizational/workplace safety

1. Introduction

The great potential and benefits of human-robot collaboration (HRC) are becoming increasingly evident in industrial communities that are influenced by a shift from mass production to highly customised, low volume manufacturing processes [1]. Collaborative robots can automatise repetitive and high-effort tasks and can reduce human task load by providing physical assistance [2], and therefore may potentially improve the working conditions of human workers. On the other hand, humans have better cognitive capability and can therefore supervise robots' operation or transfer new skills to the collaborative robot [3, 4] thus adding a certain level of flexibility to the process and contributing to effective accomplishment of a broad range of manufacturing tasks.

One of the most evident problems that arises from the integration of the human co-worker into the robot's workspace is human safety. Ensuring a safe interaction between the human and robot counterparts should be the main prerequisite of any collaborative robot control. The prominent examples of such safety strategies are collision detection and reactive motion planning techniques [5, 6, 7, 8, 9, 10], to avoid physical contacts between the robots and humans. Other approaches explore the use of compliance control strategies [11, 12] to limit impact forces [13, 14, 15, 16], or robots skins [17, 18] to detect physical contacts and react accordingly. In this direction, a concept of safety map was recently introduced to give the controller the information about human injury occurrence and inherent global or task-dependent safety properties of a robot in a unified manner [19, 20]. Furthermore, some researchers have proposed to use expert human demonstrations in an attempt to achieve safe collaborative behaviour of the robot [21, 22, 23, 4].

*Corresponding author
Email address: wan-soo.kim@iit.it (Wansoo Kim)
[1] These authors contributed equally to this work.

While the above mentioned strategies can prevent robots from causing physical injuries to human, nevertheless, that does not mean the human will not sustain injuries that may come due to the improper task execution or working conditions. In fact, former studies have shown that several occupational injuries and illnesses are caused by the exertion of excessive physical effort and repetitive motions in lifting, pushing or pulling on objects (e.g. drill, polish tool, etc.) [24, 25, 26]. In this direction, various heuristic, experienced-based guidelines have been proposed to prevent injuries related to such work activities [27, 28], by focusing on human pose, tool or task types, and the environmental conditions. Nevertheless, most of the existing techniques to monitor human ergonomics neglect the dominant effect of interaction dynamics, which can contribute to the improvement or worsening of human ergonomics, or they do not consider robotic co-workers [29].

To improve human ergonomics in interactive scenarios, the collaborative robots must observe and track human dynamic and kinematic states using their sensory systems (see Fig. 1). However, the dynamical modelling of the human body is a very complex task [30, 31]. Such precise models may be computationally too expensive for on-line uses and are therefore limited to off-line processing [32, 26, 33]. Off-line techniques, on the other hand, lack the adaptability and may not be suitable in dynamically changing environments. Some previous work aimed at addressing the required on-line adaptability needs [34, 35, 36, 3, 37], however, only kinematic aspects of human partner were taken into account. Other methods in HRC used on-line human effort models that can approximate the dynamical aspects, such as minimum joint torque index [38] or muscle fatigue index [4, 39], with the observation only limited to the human arm and did not consider human whole-body dynamics.

To address the above-mentioned limitations, we recently proposed a method for on-line estimation of the overloading joint torques[2] in static poses of the human body [40], which relies on a dynamic model of the human and uses various real-time sensory measurements. The accuracy of the proposed model in estimation of the whole-body centre of pressure (CoP) and the overloading joint torques has been evaluated in our previous work [40]. A principled simplification of the human whole-body model enabled on-line estimation of human dynamic states. We then integrated this method into a robot control framework in HRC that enabled the

[2]The overloading joint torque refers to the torque induced into the human joint by an external load.

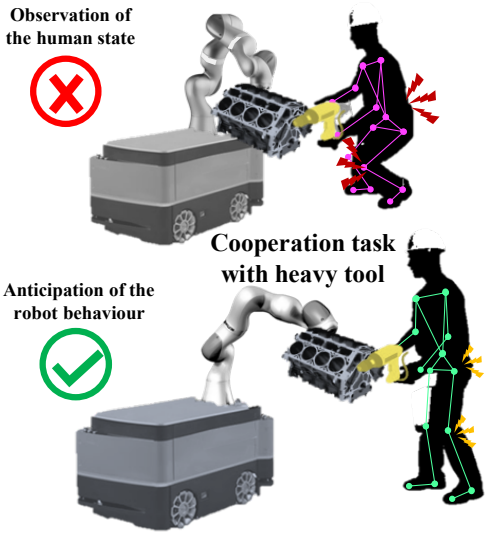

Figure 1: **The illustration of the proposed concept.** The proposed ergonomic control of human-robot collaboration aims to minimise the effect of overloading joint torques and maximise the arm manipulation ability while performing a repetitive manufacturing task.

robot to minimise the human overloading joint torques by assisting the human to work in a more suitable configuration [41]. However, one of the disadvantages of this control framework was that it still assumed static body pose of the human. More importantly, the method required measurement of ground reaction forces of the human by force plates, which can severely reduce its applicability in realistic industrial settings. In addition, the method was not able to account for some important task-dependent parameters, such as manipulability[3] of the human at hand, which can improve the effectiveness of collaboration and contribute to a better production quality.

The aim of this paper is to propose a novel human-robot collaboration control method that can guide human co-workers to more ergonomic working configurations during dexterous operations such as drilling or polishing by using a power tool. Unlike the method in [41], the proposed method does not require the ground

[3]Manipulability is a measure of an articulated mechanical structure about how the motion in joint space affects the motion of endpoint in Cartesian space, and is dependent on configuration of the structure. In case of force manipulability, the relationship is between joint torques and Cartesian wrench. Formally, scalar manipulability index is derived by determinant of Jacobian matrix as $w = \sqrt{\det(\mathbf{J}(\mathbf{q})\mathbf{J}(\mathbf{q})^T)}$, while manipulability ellipsoids are derived by singular values and vectors of Jacobian matrix.[42] For velocity manipulability it is derived as $\mathbf{U}\mathbf{\Sigma}\mathbf{V}^T = \mathbf{J}(\mathbf{q})\mathbf{J}(\mathbf{q})^T$, and for force manipulability it is derived as $\mathbf{U}\mathbf{\Sigma}\mathbf{V}^T = (\mathbf{J}(\mathbf{q})\mathbf{J}(\mathbf{q})^T)^{-1}$.

reaction force measurements during the on-line phase and is not limited to static poses[4], both of which can increase its applicability in real industrial settings. The method is considered for quasi-static cases, for typical industrial tasks in which the contributions of inertial-related elements in overloading torques are relatively small in comparison to the ones produced by the gravitational load. Furthermore, the proposed method accounts for manipulation capacity of the human at hand during the optimisation procedure. We selected the two indicators so that one of them can account for the dynamic aspects while the other can account for kinematic aspects, blending information about human dynamic loading and task performance which can contribute to reducing stress and improving productivity. Joint torque is a basic variable that describes the human effort, and reducing it would imply that the operator must provide less effort to perform a task. Meanwhile, manipulability can describe the task execution capabilities (hand velocities and forces) of the arm, and can be associated with comfort since higher manipulability would simply imply easier control of the task velocities. However, there are other indicators that can be considered and selected for the optimisation. For additional indicator selection one can refer to the related literature [43, 44].

To validate our approach, we provide detailed statistics of ten subjects in a collaborative polishing task, in which the task of the human was to operate the polishing machine, while the robot's task was to bring the object. We analysed and compared the results of human overloading joint torques in the body, human arm manipulability capacity, and measured muscle activities in the arm between six pre-selected working configurations, spread across the human arm workspace, and the optimised configuration, as obtained by the proposed method.

A preliminary study of this work was presented at 2017 IEEE-RAS International Conference on Humanoid Robotics [45]. The specific contributions of this paper that go beyond the preliminary study are: 1) considerable extension of method formulation that takes into account human muscular manipulability instead of a classic manipulability, which does not properly account for human biomechanics, 2) experiments on ten subjects supported with statistical analysis and 3) a thorough evaluation procedure.

[4]While in many industrial tasks the body remains relatively static during the task execution (e.g., polishing an object with a machine, etc.), many tasks involve some kind of arm movements that makes them dynamic.

2. Observation layer

In this section, we introduce an observation layer to monitor the human current states in real-time. This layer measures the human kinematics and uses a dynamic model of the human to estimate the overloading joint torques in the body. We first need to perform an off-line calibration to identify the subject-dependent parameters of the dynamical model, it will be explained in the human whole-body model by using the statically equivalent serial chain (SESC) technique. Once the parameters are identified, the model is used for the real-time estimation of human overloading joint torques.

2.1. Human Whole-Body Model

The proposed estimation of human overloading joint torques is based on the method we recently proposed in [41]. In this approach, the overloading joint torques are determined by the difference of CoP displacement and the ground reaction forces (GRF) relation between the condition where the effect of an external interaction force is present and where it is not present. However, one of the limitations of this approach is that it assumes a static condition of the human body. Another limitation is that it needs an external force plate to measure the CoP that is affected by the interaction force. In this paper, we extend the previous concept in order to make the estimation of the overloading joint torque in dynamic poses without using external force plate devices.

The CoP components in the dynamic condition are characterised by the differences between the acceleration about the centre of mass (CoM) and the angular momentum [46, 47]. Let $\mathbf{C}_P = [C_{Px} \quad C_{Py}]^T \in \mathbb{R}^2$ and $\mathbf{C}_M = [C_{Mx} \quad C_{My} \quad C_{Mz}]^T \in \mathbb{R}^3$ denote CoP and CoM, respectively. Let us assume that we have a whole-body, represented by a point mass. In such a model, resting on a flat ground and rotationally stable, the rate of change of spin angular momentum is considered small enough to be neglected. Thus, $\mathbf{C}_P$ can be represented as

$$\mathbf{C}_P = \begin{bmatrix} C_{Px} \\ C_{Py} \end{bmatrix} = \begin{bmatrix} C_{Mx} \\ C_{My} \end{bmatrix} - \frac{(C_{Mz} - C_{Pz})}{\ddot{C}_{Mz} + g_z} \begin{bmatrix} \ddot{C}_{Mx} \\ \ddot{C}_{My} \end{bmatrix}, \qquad (1)$$

where g_z is acceleration due to gravity, and C_{Pz} is the height of ground, which is equal to zero, since we assume that the ground is flat and is not moving with respect to Σ_W. It is noteworthy that the CoP and CoM points coincide on the support plane with the quasi-static assumption. As such, the CoP vector can be obtained by taking the CoM. We use a SESC technique [48] in order to determine the whole-body CoM of a articulated multi-body system (e.g. human). The CoM of

a model with an n number of links as

$$\mathbf{C}_M = \mathbf{x}_0 + \mathbf{B}\mathbf{\Phi}, \tag{2}$$

where $\mathbf{x}_0 \in \mathbb{R}^3$ is the position of the human floating base frame Σ_0, which is connected to the inertial frame Σ_W.

To identify the subject parameters $\hat{\mathbf{\Phi}}$, a linear system in (2) should be solved by a classical least-squares problem. To do this, measuring two components (i.e., x and y) of the $\mathbf{B}$ and ${}^0\mathbf{C}_M = \mathbf{C}_M - \mathbf{x}_0$ for p poses should be taken. Let $\mathbf{\Omega} = \begin{bmatrix} {}^0C_{1|Mx} & {}^0C_{1|My} & \cdots & {}^0C_{p|Mx} & {}^0C_{p|My} \end{bmatrix}^T$ be a $2p \times 1$ vector that is composed of the stack of measured CoM's x and y component. Similarly, $\mathbf{W}$ is a vertical concatenation of $\mathbf{B}$ matrices for p poses and $\mathbf{W}$ is of dimension $2p{\times}3(n{+}1)$. The matrix $\mathbf{W}$ is invertible by using Moore-Penrose generalised inverse as $\mathbf{W}^+ = \left(\mathbf{W}^T\mathbf{W}\right)^{-1}\mathbf{W}^T$, we then identify the SESC parameters vector $\hat{\mathbf{\Phi}}$ as (details can be found in [41])

$$\hat{\mathbf{\Phi}} = \mathbf{W}^+\mathbf{\Omega}. \tag{3}$$

As a consequence, we can obtain a real-time estimation of CoP vector $\hat{\mathbf{C}}_P \in \mathbb{R}^2$ from (1) using an on-line estimation of the human CoM $\hat{\mathbf{C}}_M$, as well as its acceleration. The estimated subject-specific SESC parameters during an off-line calibration phase in (3) are used in (2) to obtain the on-line CoM model. The acceleration of the CoM vector is then calculated by using the Kalman filtering approach [49].

The basic strategy of the previous approach to estimate the overloading joint torques is to use the model-estimated whole-body CoP $\hat{\mathbf{C}}_{P_{wo}}$ and the measured CoP $\mathbf{C}_{P_{wt}}$ in conditions with or without the effect of external forces [41]. However, in this case, external sensory devices (e.g., force plate, sensor insoles) are required which would hinder the applicability. An extension of this approach considers to increase the applicability in realistic scenarios (e.g., industrial setting) that eliminates the requirement of using extra sensory systems.

In this paper, we propose an extension of SESC parameters that addresses the presence of an external object/tool (e.g., tool, machine, etc.) that is being manipulated by the human. The contribution of this extension can update the human CoP model to include an external object/tool, it is able to obtain the CoP in real-time instead of measuring it. Such an approach can be applied in cases when the robot can either estimate the parameters of unknown object/tool (e.g., measurement by its own sensory system as the force/torque sensor, torque sensor, etc.), when objects/tools are estimated by the perception system according to the predefined tool database (e.g., detect by the vision system, etc.).

The modified SESC parameters refer to the new mass distribution of a branch where the external object/tool is manipulated. Let $\overline{\mathbf{\Phi}} = \begin{bmatrix} \overline{\boldsymbol{\phi}}_0^T & \cdots & \overline{\boldsymbol{\phi}}_n^T \end{bmatrix}^T$ be a $3(n+1)\times 1$ vector of the modified SESC parameters. When the object/tool is applied to the end-point of a branch (e.g., hand, foot, etc.), the k-th modified SESC parameter, where k refers to an index of a segment within the branch (e.g., base, upper arm, and lower arm), should be updated as

$$\overline{\boldsymbol{\phi}}_k = \frac{1}{M + m_e}\left(M\boldsymbol{\phi}_k + m_e^k\mathbf{d}_{k|\text{next}}\right), \tag{4}$$

where M is the total mass represented by the sum of the whole-body link masses and m_e is the external object/tool mass. ${}^k\mathbf{d}_{k|\text{next}} \in \mathbb{R}^3$ is the link length vector of the k-th segment measured from the frame attached to k-th segment to the next segment in the engaged branch. Intuitively, the last segment of the modified SESC model can be considered by an extension of the original SESC to the additional segment as the external object/tool. Hence, the link length of the last k-th segment is obtained by CoM of the external object/tool. For example, if the the object/tool is applied to the right hand (i.e, the segment's index of right arm branch is $k \in [0, 3, 4]$), the SESC parameters of right arm will be achieved by the link length; ${}^0\mathbf{d}_{0|\text{next}}$: base to right shoulder; ${}^3\mathbf{d}_{3|\text{next}}$: right shoulder to right elbow; ${}^4\mathbf{d}_{4|\text{next}}$: right elbow to CoM position of the external object/tool.

Using the real-time CoP estimation function (1), the CoP with externally loaded condition $\hat{\mathbf{C}}_{P_{wt}}$ is calculated by using the extended model $\overline{\mathbf{\Phi}}$ from (4) in (2).

2.2. The Overloading Joint Torque

In the proposed method, the floating base human model is used in a way that each link of human is articulated through n revolute joints, whose locations are defined by a local reference frame Σ_i at the corresponding joint. The pelvis link is selected as a base frame Σ_0. The system configuration is represented as $\mathbf{q} = \begin{bmatrix} \mathbf{x}_0^T & \boldsymbol{\theta}_0^T & \mathbf{q}_h^T \end{bmatrix}^T \in \mathbb{R}^{6+n}$, where $\mathbf{x}_0 \in \mathbb{R}^3$ and $\boldsymbol{\theta}_0 \in \mathbb{R}^3$ are the position and orientation of Σ_0 with respect to Σ_W, while $\mathbf{q}_h$ are angular positions of n human joints. The spatial velocity of the base frame can be expressed as $\boldsymbol{\vartheta}_0 = \begin{bmatrix} \boldsymbol{v}_0^T & \boldsymbol{\omega}_0^T \end{bmatrix}^T \in \mathbb{R}^6$, where $\boldsymbol{v}_0$ and $\boldsymbol{\omega}_0$ correspond to linear and angular velocities, respectively. $\dot{\mathbf{q}}_h$ is the joint velocities vector. Hence, the velocity of the system is represented by $\boldsymbol{\vartheta} = \begin{bmatrix} \boldsymbol{\vartheta}_0^T & \dot{\mathbf{q}}_h^T \end{bmatrix}^T \in \mathbb{R}^{6+n}$. The dynamic relationship between the body motion and

external forces at various contact points is given as

$$\mathbf{M}(\mathbf{q})\dot{\boldsymbol{\vartheta}} + \mathbf{C}(\mathbf{q}, \boldsymbol{\vartheta})\boldsymbol{\vartheta} + \mathbf{G}(\mathbf{q}) = \mathbf{S}^T\boldsymbol{\Gamma} + \sum_{i=1}^{n_k} \mathbf{J}_{p_i}^T(\mathbf{q})\mathbf{F}_i, \quad (5)$$

where $\mathbf{M}(\mathbf{q})$, $\mathbf{C}(\mathbf{q}, \boldsymbol{\vartheta})$, and $\mathbf{G}(\mathbf{q})$ represent the inertia matrix, vector of centrifugal and Coriolis forces, and vector of the gravity force, respectively. $\mathbf{S} = [\mathbf{0}_{n\times 6} \quad \mathbf{I}_{n\times n}]$ is a selection matrix for the actuated joints and $\boldsymbol{\Gamma}$ is the $n \times 1$ vector of applied joint torques. $\mathbf{J}_{p_i}(\mathbf{q})$ is the Jacobian of the contact constraints $\mathbf{p}_i$, where the n_k number of constraint contact wrenches $\mathbf{F}_i$ are applied with respect to Σ_W. Such a Jacobian matrix $\mathbf{J}_{p_i}(\mathbf{q}) = \begin{bmatrix}\mathbf{J}_{p_i}^b(\mathbf{q}) & \mathbf{J}_{p_i}^r(\mathbf{q})\end{bmatrix}$ reveals the contribution from the passive chain for the floating base and the actuate joints on the branch where $\mathbf{J}_{p_i}^r(\mathbf{q})$ corresponding to the displacement of joints on the contact point with respect to the base frame Σ_0.

The overloading joint torques are calculated from the difference between the joint torques calculated in conditions with and without the external forces. Due to the external load, the CoP is also displaced compared to the CoP in the unloaded condition. Similarly to (5), the torque vector in condition without the external force $\boldsymbol{\Gamma}_{wo}$ is expressed by using estimated whole-body CoP $\hat{\mathbf{C}}_{P_{wo}}$ from the original SESC parameters in (3) as

$$\mathbf{S}^T\boldsymbol{\Gamma}_{wo} = \boldsymbol{\Gamma}_b - \sum_{i=1}^{n_f} \mathbf{J}_{\hat{C}_{P_{wo}i}}^T(\mathbf{q})\mathbf{F}_{i|wo}, \quad (6)$$

where $\boldsymbol{\Gamma}_b \in \mathbb{R}^{n+6}$ corresponds to the left part of (5), which is the joint torque vector of human body without the contact constraints (e.g., ground contact, hand contact, etc.). Due to the assumption on the quasi-static movement of the human body, the velocity and acceleration of the system are close to zero ($\dot{\boldsymbol{\vartheta}} = \boldsymbol{\vartheta} \cong 0$), thus on the contribution of the gravity term in the left part of (5) is considered. $n_f \in \{1, 2\}$ is the number of ground contact points at the foot. The vertical GRF (vGRF) $\mathbf{F}_{wo}$, which is obtained from the human body mass, act on the human body by the transpose of the Jacobian as $\mathbf{J}_{\hat{C}_{P_{wo}i}}^T(\mathbf{q})\mathbf{F}_{i|wo}$ at the point of estimated CoP $\hat{\mathbf{C}}_{P_{wo}i}$.

On the other hand, the condition with the external object/tool produces a torque $\boldsymbol{\Gamma}_{wt}$, which is calculated by using $\hat{\mathbf{C}}_{P_{wt}}$ from the modified SESC parameters as

$$\mathbf{S}^T\boldsymbol{\Gamma}_{wt} = \boldsymbol{\Gamma}_b - \sum_{i=1}^{n_f} \mathbf{J}_{\hat{C}_{P_{wt}i}}^T(\mathbf{q})\mathbf{F}_{i|wt} - \sum_{j=1}^{n_h} \mathbf{J}_{a_{hj}}^T(\mathbf{q})\mathbf{F}_{j|h}, \quad (7)$$

where $\mathbf{F}_{wt}$ is the vGRF vector applied at $\hat{\mathbf{C}}_{P_{wt}}$ in this condition that is obtained from the combined mass of the human body and the external object/tool. $\mathbf{F}_h$ represents the pre-estimated mass of the object/tool that are applied at the contact points $\mathbf{a}_h$. $\mathbf{J}_{\hat{C}_{P_{wt}i}}(\mathbf{q})$ and $\mathbf{J}_{a_{hj}}(\mathbf{q})$ refer to the contact Jacobian at the point of $\hat{\mathbf{C}}_{P_{wt}i}$ and $\mathbf{a}_{hj}$, respectively. $n_h \in \{1, 2\}$ is the number of operated hands where the tools/objects are handled.

Consequently, the overloading joint torques are defined by the difference between the torque vectors from (6) and (7) as

$$\mathbf{S}^T\Delta\boldsymbol{\Gamma} = \sum_{j=1}^{n_h} \mathbf{J}_{a_{hj}}^T(\mathbf{q})\eta_j\Delta\mathbf{F} - \sum_{i=1}^{n_f}\Big((\mathbf{J}_{\hat{C}_{P_{wt}i}}^T(\mathbf{q}) - \mathbf{J}_{\hat{C}_{P_{wo}i}}^T(\mathbf{q}))\mathbf{F}_{i|wt} + \mathbf{J}_{\hat{C}_{P_{wo}i}}^T(\mathbf{q})\zeta_i\Delta\mathbf{F}\Big), \quad (8)$$

where $\Delta\mathbf{F} = \sum_{i=1}^{n_f}\Delta\mathbf{F}_{i|w} = -\sum_{j=1}^{n_h}\mathbf{F}_{j|h}$ is the sum of the interaction forces. As regards the distribution gain ($\sum_i \zeta_i = 1$ and $\sum_j \eta_j = 1$) related to the number of contact points, we can consider that the gain is defined by the employed human model; for example, if the model is interacting with environment using a single arm and single foot, hence $\eta = 1$ and $\zeta = 1$. A further example of the multi-interaction model has been reported in [50] where the model assumes a symmetric distribution of the grasp forces in two hands while carrying an object ($\eta_j = 0.5$), but the force distribution on the feet (ζ_i) is computed by the synergistic model approach in real-time.

3. Anticipation layer

This section introduces an anticipation layer[5] that is used by the robot to predict the optimal configuration of task execution to accommodate ergonomic working conditions for the human co-worker. This layer relies on the observation layer (see Fig. 2) to obtain the desired configuration of the task execution through a constrained optimisation technique that reduces the joint torque variation of human under several constraints. In particular, we used the human arm muscular manipulability as a constraint in this optimisation to facilitate the human movements in achieving a good manipulation capacity in the optimised configuration.

3.1. Optimisation

Here we present the minimisation procedure of human overloading joint torque vector with respect to body configuration and given constraints. This consideration was to avoid potential injuries caused by the excessive loading effect during the execution of a collaborative task.

[5]The "anticipation" refers to the ability of the method to anticipate overloading joint torques and then react to minimise them.

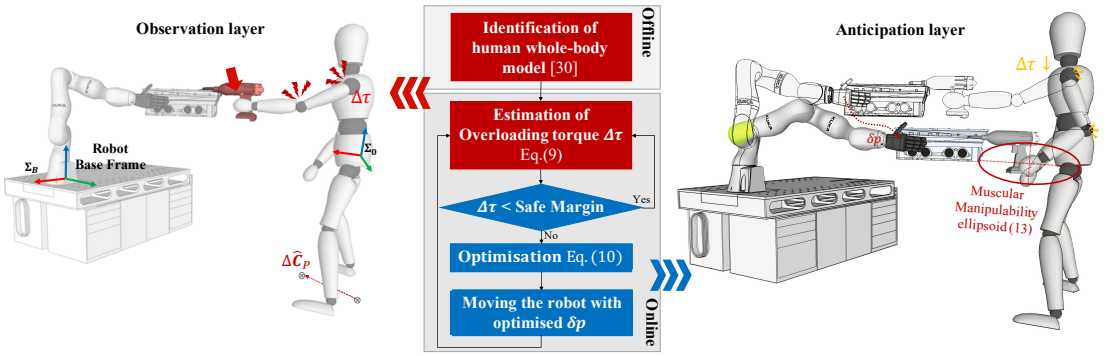

Figure 2: **The overall procedure of the proposed method.** The observation (left) and the anticipation layer (right) for estimating and reducing the overloading joint torques in human-robot collaboration are illustrated.

The optimisation problem can be designed to minimise the sum of the weighted norms of the overloading joint torques, which is represented by the human joint state variable $\mathbf{q}_h$, subject to nonlinear inequality constraints

$$\min_{\mathbf{q}_h} f(\mathbf{q}_h) = \frac{1}{2}\sum_{k=1}^{n} w_k \left\|\Delta\boldsymbol{\Gamma}_k(\mathbf{q}_h)\right\|^2, \tag{9}$$

$$\text{subject to: } \mathbf{q}_L \leq \mathbf{q}_h \leq \mathbf{q}_U, \tag{10}$$

$$\mathbf{h}_{\text{stable}}(\mathbf{q}_h) \leq 0, \tag{11}$$

$$\mathbf{h}_{\text{share}}(\mathbf{q}_h) \leq 0, \tag{12}$$

$$\mathbf{h}_{\text{Manipulability}}(\mathbf{q}_h) \leq 0, \tag{13}$$

where $\Delta\boldsymbol{\Gamma}_k(\mathbf{q}_h)$ is the k-th joint's overloading torque, which is obtained from (8), w_k is a weight associated with the joint k, and $\mathbf{h}$ are inequality box constraints. All weights ($w > 0$) per optimisation cycle are calculated by $|\Delta\boldsymbol{\Gamma}_k/\boldsymbol{\Gamma}_{\max_k}|$ and kept fixed, with $\Delta\boldsymbol{\Gamma}_k$ and $\boldsymbol{\Gamma}_{\max_k}$ representing the actual overloading torque value at the start of optimisation, and the maximum joint torque value at the k-th joint, respectively. Such weights are meant to set priorities between the joints, so that the ones that are more imposed to risks are given mote attention in the quadratic optimisation process. For instance, $\Delta\boldsymbol{\Gamma}_k \approx \boldsymbol{\Gamma}_{\max_k}$ implies that that the k-th joint has a higher injury risk, and should get the highest priority via $w_k \approx 1$ in comparison to other joints during the optimisation. The tuning and personalisation of the maximum joint torque values were based on experiments on subjects, where we applied increasing torque profiles on selected body joints, one at a time. This was done until a subject stated to feel uncomfortable around that joint. In that particular moment, the resulting torque values were estimated (based on the applied force and the lever arm) and compared to the ones extracted from literature (see the work by Snook and Ciriello [51]). If these values were comparable, we used the experimental ones as the maximum torque values. If the differences were large, the "safest" choice, i.e., the smallest value for the maximum torque, was chosen.

In the optimisation process, we consider several constraints. To ensure a safe configuration after the optimisation, (10) expresses a boundary condition of the human joint angles, which are constrained within the human body joint limitations represented by lower $\mathbf{q}_L$ and upper $\mathbf{q}_U$ boundaries. Further constraints arise from the postural stability. (11) as a set of inequality constraints is considered so that the position of CoP only exists within convex hull of the contact points (i.e. within the support polygon of feet). Thus, the inequality constraint (11) is formulated as

$$\mathbf{h}_{\text{stable}}(\mathbf{q}_h) := \hat{\mathbf{C}}_{P_{wt}}(\mathbf{q}_h) - \text{conv}\{\boldsymbol{p}_{F|i}^{x,y}\} \leq 0, \tag{14}$$

where $\hat{\mathbf{C}}_{P_{wt}}(\mathbf{q}_h)$ is the CoP estimation model as shown in (1), $\text{conv}\{\boldsymbol{p}_{F|i}^{x,y}\}$ is the convex hull of the contact points that can be computed by the forward kinematic of the feet.

(12) expresses the inequality constraint to represent the proxemics space. The box constraint sets the object position within the threshold not only as the maximal distance from the human base frame but also as the maximal distance from the robot base, so that the co-manipulated object is constrained within the feasible shared workspace of the human and the robot. To do this, the inequality constraint (12) is defined by

$$\mathbf{h}_{\text{share}}(\mathbf{q}_h) := \begin{cases} \boldsymbol{p}_{obj}(\mathbf{q}_h) - \boldsymbol{p}_{H|th} \leq 0, \\ -(\boldsymbol{p}_{obj}(\mathbf{q}_h) - \boldsymbol{p}_{R|th}) \leq 0, \end{cases} \tag{15}$$

where $\boldsymbol{p}_{R|th}$ and $\boldsymbol{p}_{H|th}$ are the position threshold of the robot side and the human side, respectively. The thresholds for the shared workspace are defined by the limits

of intersection of human and robot workspaces, where each is calculated by respective forward kinematics. $\boldsymbol{p}_{obj}(\mathbf{q}_h)$ is the targeted object's position, which is calculated by the forward kinematics. Each thresholds and the object's position are represented in the base frame, therefore, the constraints should be represented within the shared Cartesian workspace The application of such constraints in the optimisation process ensures the stability and safety of the human co-worker and the collaboration task.

The final constraint in (13) is the endpoint manipulability of the human arm. In general, humans adjust the configuration of their body and limbs in order to maximise the kinematic and dynamic properties according to given tasks and environmental conditions [52]. In robotics, the classic measure for the kinematic and dynamic properties of a robot end-effector is the *manipulability*, which provides an idea of how well the end-effector can produce velocity or force in different directions of the Cartesian space [42]. Manipulability can be geometrically represented as an ellipsoid at the end-effector, whose radius in a specific direction indicates the velocity/force production ability. In a specific example, if the task requires that the object/tool is manipulated in a complex manner, which involves production of end-effector force and velocity equally in various directions of Cartesian space, the configuration of the arm should be maintained close to where endpoint manipulability ellipsoid is isotropic. Nevertheless, the classic manipulability, which has been extensively studied in the robotic manipulators actuated by electric motors, is not able to faithfully measure the manipulation ability of the human body. This is because the human body is actuated by the muscles that have spring-like properties and antagonistically pull the joint in different directions. Therefore, it is necessary to account for the effect of this specific feature of human actuators on the endpoint manipulability. To do so, we include *muscular manipulability* [53, 54] in the proposed optimisation process as a constraint condition. Hence, in our work, the position of the object/tool being co-manipulated is also constrained by the human arm muscular manipulability.

The relation between the muscle forces and the endpoint force is defined as

$$\mathbf{F} = \mathbf{J}_a^{+T}(\mathbf{q}_a)\mathbf{J}_m^{T}(\mathbf{q}_a)\mathbf{F}_m, \tag{16}$$

where $\mathbf{F}$ is endpoint force, which can be one of the external contact wrenches from (5), $\mathbf{q}_a \in \mathbf{q}_h$ is joint angle vector of arm, $\mathbf{J}_a^{+}(\mathbf{q}_a)$ is Moore–Penrose inverse of the geometric Jacobian matrix of arm, $\mathbf{J}_m(\mathbf{q}_a)$ is muscle Jacobian matrix that contains muscle moment arms at the joints, and $\mathbf{F}_m$ is muscle force, which we calculate by using the Hill's muscle model

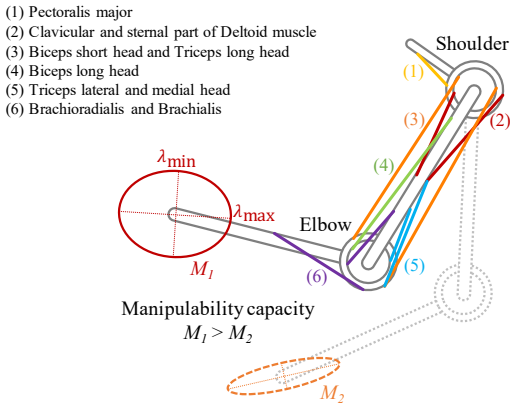

Figure 3: **Ten muscles are considered in the definition of arm manipulability capacity.** The resulting ellipsoid and its major and minor axes are conceptually illustrated in this figure.

$$\mathbf{F}_m = \mathbf{F}_{hill}\boldsymbol{\alpha}, \tag{17}$$

where $0 \leq \boldsymbol{\alpha} \leq 1$ muscle activation and $\mathbf{F}_{hill}$ is a diagonal matrix representing the Hill's muscle force.

By combining (16) and (17), the muscular manipulability is obtained from expression $(\mathbf{J}_a^{+T}(\mathbf{q}_a)\mathbf{J}_m(\mathbf{q}_a)\mathbf{F}_{hill})$ that transforms muscle activations to Cartesian endpoint force. Unlike classic manipulability measure that considers only geometric Jacobian $\mathbf{J}_a(\mathbf{q}_a)$, muscular manipulability takes into account also muscle Jacobian $\mathbf{J}_m(\mathbf{q}_a)$. Assuming $\|\boldsymbol{\alpha}\| < 1$, we can derive the expression to obtain the manipulability (see [54] for details)

$$\mathbf{K}(\mathbf{q}_a) = (\mathbf{J}_a^{+T}(\mathbf{q}_a)\mathbf{J}_m(\mathbf{q}_a)\mathbf{F}_{hill})(\mathbf{J}_a^{+T}(\mathbf{q}_a)\mathbf{J}_m(\mathbf{q}_a)\mathbf{F}_{hill})^T. \tag{18}$$

By applying singular value decomposition of $\mathbf{K}(\mathbf{q}_a)$ we obtained the eigenvalues λ that represent the axial lengths of the endpoint manipulability ellipsoid. Consequently, the manipulability capacity $M(\mathbf{q}_a) = \frac{\lambda_{\min}(\mathbf{K}(\mathbf{q}_a))}{\lambda_{\max}(\mathbf{K}(\mathbf{q}_a))}$ was defined as a ratio between the minimum and the maximum eigenvalue. For our experiments we normalised this value, $\tilde{M}(\mathbf{q}_a)$ to the maximum ratio of the entire workspace, which gave us a percentage value. A higher value of manipulability capacity indicates that the capacity to produce the arm endpoint force and velocity is better in all directions of the Cartesian space.

Our arm model included two segments and two joints (3 DoF in the shoulder and 1 DoF in the elbow). We considered ten muscles (see Fig. 3): clavicular and sternal part of Deltoid muscle (shoulder), Pectoralis major (shoulder), Biceps short head and Triceps long head

(bi-articular), Biceps long head (elbow), Triceps lateral and medial head (elbow), Brachioradialis (elbow) and Brachialis (elbow).

To ensure good manipulability in all directions of human arm endpoint, (13) was defined a certain degree of manipulability capacity as an inequality constraint:

$$\mathbf{h}_{\text{Manipulability}}(\mathbf{q}_h) := \tilde{M}_{th} - \tilde{M}(\mathbf{q}_a) \leq 0, \qquad (19)$$

where $\tilde{M}_{th}$ is the manipulability capacity constraint. The method therefore searched for the optimal minimum overloading joint torques within configurations, where the manipulability ellipsoid was close to isotropic. The optimisation problem of (9) was used to formulate a nonlinear programming problem, which was then solved using the active set method of the ALGLIB optimisation library.

3.2. Execution of the robot behaviour

To achieve a more ergonomic working condition of the human co-worker, the robot uses the optimised configuration of the human body obtained through (9). Using the forward kinematics, the current human configuration and the optimised one are expressed in Cartesian space. The difference between the two is used to calculate the robot end-effector trajectory, which brings the human from the current to the optimised configuration.

To achieve safe and adaptive interaction between the human and robot, the Cartesian impedance controller by default was set the stiffness parameter to 1500 N/m in the translational axis and 150 Nm/rad in the rotational axis, respectively. These values provided a reasonable trade-off between the trajectory tracking performance and the end-effector compliance. The human partner was simultaneously provided with a visual feedback regarding the optimised configuration, which made sure that the correct configuration was maintained.

4. Experimental Evaluation

Ten healthy male volunteers (age: 27.6 ± 2.3 years; mass: 75.1 ± 5.3 kg; height: 1.80 ± 0.03 m)[6] were recruited for this study. The experiments were performed at HRI^2 Lab of IIT, Italy. The study was approved by the Regional Ethics Committee of Liguria (IIT_HRII_001, 108/2018).

First, we obtained the data for identification of dynamic model (i.e., SESC parameters) of each subject.

[6]Subject data is reported as: mean ± standard deviation.

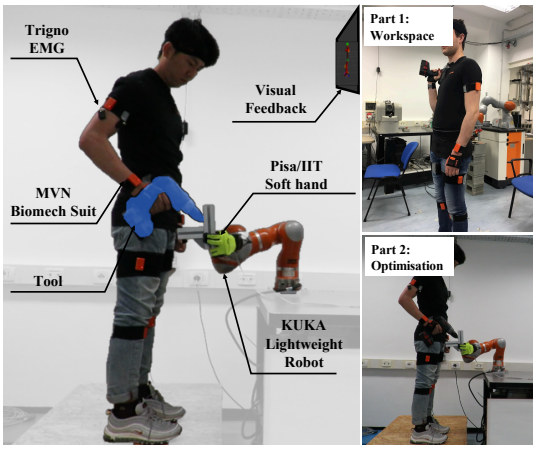

Figure 4: **Overview of the experimental setup.** The experimental setup consisted of a MVN Biomech suit, a KUKA LBR IV+ equipped with the Pisa/IIT softhand, visual feedback and wireless EMG sensors. The experimental purpose consisted of two parts: task comparison in workspace of the arm, and evaluation in the optimisation.

The subjects wore the MVN Biomech suit (Xsens Technologies BV) and stood on a Kistlter force plate. They were asked to perform 140 different static configurations of their body, then we selected $p = 21$ linearly-independent poses to identify the SESC parameters vector $\hat{\mathbf{\Phi}}$ in (3). Note that the force plate is required only during the off-line calibration and is not required during the on-line phase.

The experimental setup is illustrated in Fig. 4. The subjects wore the MVN Biomech suit to measure the body configuration in real-time. The experimental evaluation involved a human-robot collaboration task. In this scenario, the robot held an object that had to be polished by the human subject, who used a heavy hand-held tool (mass: 3.4 kg). To do this, we developed a simplified human body model with five joints (i.e., hip, knee, ankle, shoulder and elbow), which primarily contributed to Sagittal plane motion. Additionally, such a model was interacting with environment using a single hand and foot, hence, the contribution gain of hand and foot were $\eta = 1$ and $\zeta = 1$, respectively.

The task of the robot was to bring the object to the human, while the task of the human was to polish it[7]. In such a task, the robot should adapt its behaviour in a way that the working conditions are improved for the human co-worker, which signifies that any excessive

[7]This scenario can be generalised to other collaboration tasks (e.g., drilling, assembly, etc.) and handover tasks. For example, in the handover task the robot brings the object to the human, who then takes it from the robot at a certain position.

joint load is prevented and the arm manipulability capacity value is maximised.

The whole-body configuration should ideally be in a pose where the overloading joint torques are as low as possible, while achieving a high arm manipulability capacity to facilitate an effective task execution. In the experiments, the arm manipulability capacity constraint was set to 80% of maximum capacity, which was obtained by scanning through the feasible arm workspace for each subject. This led to a good force and velocity production capacity in all directions since the human arm endpoint at the manipulation location had close-to-isotropic manipulability ellipsoid. The time required to scan through the feasible arm workspace for each subject was 87 seconds. However, this scanning process needs to be conducted only once for each subject and the result can be reused in future.

When performing tasks like polishing, there is some deviation from the optimal position. During the experiment we assumed that the task execution movement is within a close proximity of the optimised solution and that these deviation are small. However, if considerable deviations are necessary to perform the task, re-optimisation is required.

The experimental procedure was divided into two stages (as shown in the right of the Fig. 4). In the first stage, the subjects had to perform the given task in six different configurations of the arm, following the outline of the range of risk in the shoulder and elbow on Rapid Entire Body Assessment (REBA) [55]. See Fig. 5 for details and illustrations of the selected configurations. In the second stage, the proposed method was used to select the optimal working configuration in terms of overloading joint torques and given constraints (manipulability capacity, etc.). The on-line acquisition of the human body position data was performed using the MVN Biomech system. This data was then used to calculate vector $\mathbf{x}_0$ and matrix $\mathbf{B}$ that were necessary for real-time calculation of CoP in (2) and the human overloading joint torque vector in (8).

To compare the arm muscular effort during the task execution in an optimised configuration and six predefined ones, we recorded and evaluated the muscle activity from electromyography (EMG) measurements. For the EMG measurements, we selected Anterior Deltoid (AD), Posterior Deltoid (PD), Biceps Brachii (BB) and Triceps Brachii (TB), which are the dominant shoulder and elbow muscles in the given configurations. The EMG signals were acquired using Delsys Trigno Wireless system, and processed by full rectification, low-pass filtering, and normalisation with respect to the maximal voluntary contraction to account for muscular activities. We followed SENIAM[56] recommendations for EMG electrode placements and [57] for MVC procedures. It is important to note here that, the processed EMG signals were not used as inputs to our model, but to provide additional means of verifying the results of this study.

4.1. Results

The results of experiments are shown in Table 1, where we report the overloading joint torques, manipulability capacity value and muscle activity as measured by EMG. These variables were averaged across the subjects for each configuration. Fig. 6 shows summed mean values of overloading joint torques for different configurations. The mean manipulability capacity value for each configuration is presented in Fig. 7. The muscle activity capacity of the arm is shown in Fig. 8.

To test the statistical differences between the optimised configuration and the predefined ones, Bonferroni correction test with post-hoc t-tests was used. The level of statistical significance used was .05 for all statistical tests. The configurations 1, 4 and 6 had overall lower overloading joint torque in the body than the optimised configuration. The difference was 21.73±2.17[8] Nm (p <.001), 23.70±2.19 Nm (p <.001) and 35.50±1.48 Nm (p <.001), respectively. Even though the torque was lower in these configurations compared to the optimised configuration, the manipulability capacity was relatively low in all three compared to the optimised one. The difference was 55.31±2.19 % (p <.001), 60.65±5.59 % (p <.001) and 83.62±2.10 % (p <.001), respectively. There were statistically significant differences in all values. On the contrary, configurations 2, 3, and 5 had higher overloading joint torque than the optimised configuration. The differences were 33.82±1.49 Nm (p <.001), 8.62±1.68 Nm (p <.001) and 10.66±1.21 Nm (p <.001), respectively. In addition, the manipulability capacity in these configurations was on average much lower. The difference was 85.94±2.17 % (p <.001), 41.28±4.77 % (p <.001) and 30.76±2.77 % (p <.001), respectively. There were statistically significant differences in all values.

The measured muscle activity capacity in the human arm is shown in Fig. 8. The arm muscle activity in configurations 1, 2 and 3 was relatively high in comparison to the optimised configuration. The difference was 8.47±2.74 % (p =.017), 32.88±7.25 % (p =.0020) and 7.91±2.74 % (p =.023), respectively. The differences were statistically significant. On the other hand,

[8]The data is reported as: mean ± standard error of mean.

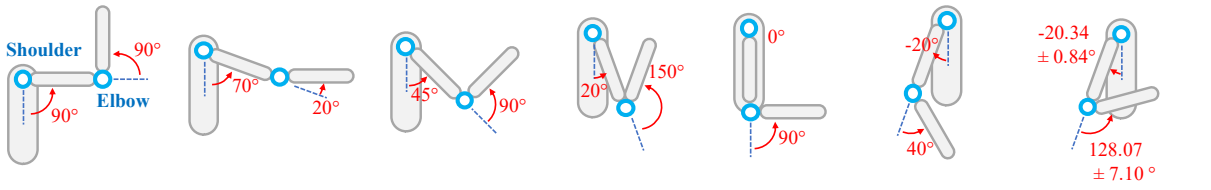

Configuration 1 (A) | Configuration 2 (B) | Configuration 3 (C) | Configuration 4 (D) | Configuration 5 (E) | Configuration 6 (F) | Optimal configuration (G)

Figure 5: **The six different unoptimised configurations and the optimised configuration.** The optimal configuration was slightly different among ten subjects, therefore the joint angle values are reported as: mean ± std.

Table 1: **Experimental results of ten subjects.** The results are separated according to seven different configurations. The data is reported as: mean (standard error of mean)[9]. Note that the optimal configuration was slightly different among the subjects.

Configuration		**1** (Fig. 5A)	**2** (Fig. 5B)	**3** (Fig. 5C)	**4** (Fig. 5D)	**5** (Fig. 5E)	**6** (Fig. 5F)	**Optimal** (Fig. 5G)
Manipulability capacity [%]		37.24*** (1.46)	6.60*** (1.00)	51.26*** (5.76)	31.89*** (5.20)	61.78*** (3.29)	8.92*** (0.79)	92.54 (1.19)
Overloading joint torque [Nm]	Hip	7.88*** (0.67)	21.25*** (0.60)	15.20** (0.550)	7.48*** (0.69)	15.37*** (0.46)	4.16*** (0.35)	13.00 (0.46)
	Knee	8.57*** (0.73)	21.67*** (0.62)	15.72** (0.55)	8.03*** (0.66)	15.89*** (0.46)	4.73*** (0.35)	13.35 (0.46)
	Ankle	9.57*** (0.78)	22.52*** (0.69)	16.61** (0.60)	8.93*** (0.72)	16.71*** (0.49)	5.56*** (0.35)	14.15 (0.54)
	Shoulder	6.99 (0.30)	15.68*** (0.25)	11.23*** (0.17)	5.72** (0.28)	9.63*** (0.20)	1.45*** (0.26)	7.11 (0.26)
	Elbow	0.52*** (0.13)	8.78** (0.14)	5.67*** (0.15)	1.98*** (0.31)	8.86** (0.14)	3.28*** (0.22)	8.25 (0.17)
Muscle activity [%]	AD	42.61*** (8.65)	80.97*** (15.48)	48.25*** (8.90)	13.92*** (2.54)	10.46*** (1.94)	4.95 (2.04)	3.59 (0.72)
	PD	18.19** (4.13)	50.54* (14.11)	10.87 (2.48)	2.98* (0.48)	2.85* (0.53)	21.49** (4.01)	7.65 (2.04)
	BB	2.28*** (0.48)	18.06 (2.37)	8.44* (1.26)	15.10 (2.64)	13.87 (2.13)	5.38** (0.63)	15.60 (2.74)
	TB	16.75 (3.39)	27.88 (4.89)	10.01* (1.73)	17.35 (3.50)	10.46* (1.78)	7.86** (1.45)	19.09 (3.23)

the muscle activity in configurations 4, 5 and 6 was comparable to optimised configuration. The difference was 0.85±1.39 % (p =.58), 2.07±1.21 % (p =.14) and 1.56±1.65 % (p =.40), respectively. The differences were statistically insignificant.

5. Discussion

From the results of overloading joint torques in different configurations, we can see that some of the tested configurations have overall lower torque in the body while performing the task. Even though the overall lower overloading joint torque would be more comfortable for the human worker, these configurations had significantly lower manipulability capacity of the arm, which could affect the task production. Since we specified a certain required degree of manipulability capacity in the optimisation process, the optimised configuration was constrained to the cases where the manipulability was above the prescribed threshold. If such high manipulability capacity is not required, the optimisation could search within other configurations where overloading joint torques can be lower. The parameters of the proposed method, such as the required manipulability capacity, the constraints on configuration of body and the orientation of endpoint/tool, should therefore be

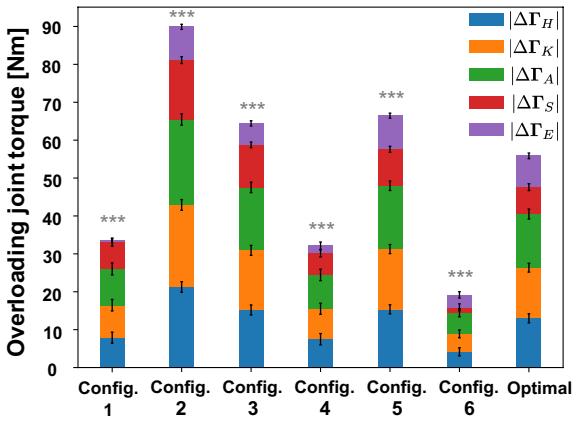

Figure 6: **The sum of all overloading joint torques for different configurations**[9]**.** Different colours in the bar represent different contribution from different joints (H: hip, K:knee, A:ankle, S:shoulder, E:elbow).

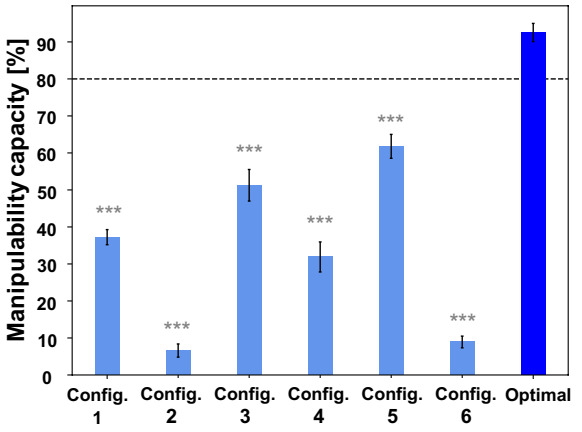

Figure 7: **The results**[9] **of the manipulability capacity for different configurations.** The black dashed line denotes the manipulability capacity constraint set in the optimisation process.

selected based on the desired industrial task [25].

The results of the arm muscle activity in configurations 4, 5, 6 and the optimised configuration were comparable besides the human worker would be more comfortable in terms of muscular effort. However, it should be noted that the muscle activity measurement was limited to the human arm, while optimisation of the overloading joint torques considered the whole body. Consequently, the overloading joint torque approach provides a good compromise between human efforts and task execution capabilities.

[9]Asterisks indicate the level of statistical significance after post-hoc tests: $^{*}p$ <.05, $^{**}p$ <.01 and $^{***}p$ <.001

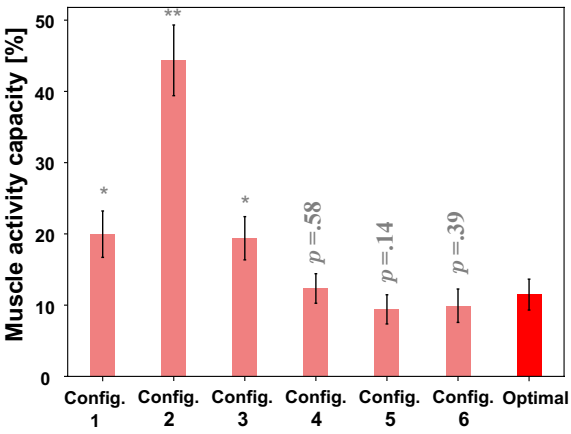

Figure 8: **The results**[9] **of the muscle activity capacity of the arm for the different configurations.** The corresponded values are defined as a summation of subject-average muscle activations of all measured muscles, normalised by the number of muscles. This value represents the percentage of combined capacity of all four measured muscles.

The main advantage of the proposed method is in its reduced complexity and limited amount of required measurement systems, which could significantly improve its applicability in real industrial environments. Further reduction of the complexity can be achieved by using more affordable motion capture systems (e.g., Microsoft Kinect). However, some of the more affordable hardware might not be suitable for all kinds of industrial settings and tasks. The framework offers flexibility not only in terms of selecting the desired amount of DoF of human body, which is easily modifiable based on the desired complexity, but also adaptation to the kinematic specifics of a task (e.g. changing tools, switching hands). Furthermore, task constraints can be modified based on the target task objectives, e.g., to impose constraints on dual-arm manipulability, etc.

The objective of the proposed method is to minimise overloading joint torque, while other variables (i.e., manipulability, joint limits, obstacles, etc.) were selected as constraints to be guaranteed. It should be stressed that potential disadvantage of this framework is that if set too vigorously, the constraints can severely limit the solution space. If a reasonable solution is not found, the constraints has to be loosened up, which might involve an expert intervention. The manipulability could also be used as an objective rather than as a constraint. Using it as a constraint may lead to an absence of solution, however if the solution is found the manipulability is within the desired range. On the other hand, using it as an optimisation objective makes it less limiting on the number of possible solutions, however it does not guarantee that

the manipulability will be in the desired range. This tradeoff should be considered when selecting between the two options.

We should stress that the proposed optimisation problem is not directly related to governing of human motion, i.e., it is not an optimisation that would be used in a human motion control problem. The proposed optimisation problem is related to finding an optimal quasi-static working posture of human that the collaborative robot can use as a recommendation by changing the working configuration. The human then has to use its own motor control to govern his/her motion around the recommended posture.

In the existing study we considered only manipulability of the arm since in common industrial tasks, e.g. using a machine to polish an object, the body is primarily used to position the shoulder joint before the task is performed and then it remain relatively static, while the arm is doing majority of the movement required to perform the task. However, if the tasks require large movements of the body, the proposed manipulability measure can be extended to the body.

While humans mostly use arm movements to perform various tasks, the external load is still distributed among the whole body. That is why we consider manipulability only for arm, but the joint torque reduction considers the whole body. For example, even if the body remains static while the arm do most of the movement with a heavy polishing machine, the load will still affect the back if the posture is not good. If the body posture as a whole is not corrected, this may lead to back pain.

In the existing study we did not consider the elastic properties of muscles, which have more dominant role in explosive movements (e.g., jumping, throwing, etc.), where the energy has to be transferred from proximal muscles to distal muscles [58, 59]. The common industrial tasks considered in this study do not involve such explosive movements and therefore we considered only antagonistic and configuration dependant nature of joint torques produced by muscles in the musculoskeletal model.

The main goal of this paper was to introduce a method that enables the robot to account for parameters related interaction dynamics during human-robot collaboration and validate the approach on multiple subjects. The future work will focus on determining to what degree the considered parameters should be accounted for and what would be the long term affects on human subjects.

Funding

This work was supported in part by the H2020-ICT-2019-2 project SOPHIA (GA 871237), European Research Council (ERC) starting grant Ergo-Lean (GA 850932) and H2020-ICT project ANDY (GA 731540).

References

[1] A. Ajoudani, A. M. Zanchettin, S. Ivaldi, A. Albu-Schäffer, K. Kosuge, O. Khatib, Progress and prospects of the human–robot collaboration, Autonomous Robots (2017).

[2] L. Gualtieri, E. Rauch, R. Vidoni, Emerging research fields in safety and ergonomics in industrial collaborative robotics: A systematic literature review, Robotics and Computer-Integrated Manufacturing 67 (2020) 101998.

[3] L. Peternel, N. Tsagarakis, A. Ajoudani, A human-robot co-manipulation approach based on human sensorimotor information, IEEE Transactions on Neural Systems and Rehabilitation Engineering 25 (2017) 811–822.

[4] L. Peternel, N. Tsagarakis, D. Caldwell, A. Ajoudani, Robot adaptation to human physical fatigue in human–robot co-manipulation, Autonomous Robots 42 (2018) 1011–1021.

[5] A. De Luca, A. Albu-Schäffer, S. Haddadin, G. Hirzinger, Collision detection and safe reaction with the DLR-III lightweight manipulator arm, in: Intelligent Robots and Systems (IROS), 2006 IEEE/RSJ Intl. Conf. on, pp. 1623–1630.

[6] D. Kulić, E. Croft, Pre-collision safety strategies for human-robot interaction, Autonomous Robots 22 (2007) 149–164.

[7] V. Magnanimo, S. Walther, L. Tecchia, C. Natale, T. Guhl, Safeguarding a mobile manipulator using dynamic safety fields, in: Intelligent Robots and Systems (IROS), 2016 IEEE/RSJ International Conference on, IEEE, pp. 2972–2977.

[8] J. Corrales, F. Candelas, F. Torres, Safe human–robot interaction based on dynamic sphere-swept line bounding volumes, Robotics and Computer-Integrated Manufacturing 27 (2011) 177–185.

[9] L. Bascetta, G. Ferretti, Ensuring safety in hands-on control through stability analysis of the human-robot interaction, Robotics and Computer-Integrated Manufacturing 57 (2019) 197–212.

[10] E. Magrini, F. Ferraguti, A. J. Ronga, F. Pini, A. De Luca, F. Leali, Human-robot coexistence and interaction in open industrial cells, Robotics and Computer-Integrated Manufacturing 61 (2020) 101846.

[11] A. Albu-Schäffer, C. Ott, G. Hirzinger, A unified passivity-based control framework for position, torque and impedance control of flexible joint robots, Int. J. Rob. Res. 26 (2007) 23–39.

[12] F. Dimeas, V. C. Moulianitis, N. Aspragathos, Manipulator performance constraints in human-robot cooperation, Robotics and Computer-Integrated Manufacturing 50 (2018) 222–233.

[13] S. Haddadin, S. Haddadin, A. Khoury, T. Rokahr, S. Parusel, R. Burgkart, A. Bicchi, A. Albu-Schäffer, On making robots understand safety: Embedding injury knowledge into control, The International Journal of Robotics Research 31 (2012) 1578–1602.

[14] B. Yao, Z. Zhou, L. Wang, W. Xu, Q. Liu, A. Liu, Sensorless and adaptive admittance control of industrial robot in physical human- robot interaction, Robotics and Computer-Integrated Manufacturing 51 (2018) 158–168.

[15] J. O. Oyekan, W. Hutabarat, A. Tiwari, R. Grech, M. H. Aung, M. P. Mariani, L. López-Dávalos, T. Ricaud, S. Singh,

C. Dupuis, The effectiveness of virtual environments in developing collaborative strategies between industrial robots and humans, Robotics and Computer-Integrated Manufacturing 55 (2019) 41–54.

[16] P. Aivaliotis, S. Aivaliotis, C. Gkournelos, K. Kokkalis, G. Michalos, S. Makris, Power and force limiting on industrial robots for human-robot collaboration, Robotics and Computer-Integrated Manufacturing 59 (2019) 346–360.

[17] J. Kim, A. Alspach, K. Yamane, 3d printed soft skin for safe human-robot interaction, in: Intelligent Robots and Systems (IROS), 2015 IEEE/RSJ Int. Conf. on, IEEE, pp. 2419–2425.

[18] G. Tang, P. Webb, J. Thrower, The development and evaluation of robot light skin: A novel robot signalling system to improve communication in industrial human–robot collaboration, Robotics and Computer-Integrated Manufacturing 56 (2019) 85–94.

[19] N. Mansfeld, M. Hamad, M. Becker, A. G. Marin, S. Haddadin, Safety map: A unified representation for biomechanics impact data and robot instantaneous dynamic properties, IEEE Robotics and Automation Letters 3 (2018) 1880–1887.

[20] A. Cherubini, R. Passama, A. Crosnier, A. Lasnier, P. Fraisse, Collaborative manufacturing with physical human–robot interaction, Robotics and Computer-Integrated Manufacturing 40 (2016) 1–13.

[21] P. Evrard, E. Gribovskaya, S. Calinon, A. Billard, A. Kheddar, Teaching physical collaborative tasks: object-lifting case study with a humanoid, in: IEEE-RAS Intl. Conf. on Humanoid Robots, pp. 399–404.

[22] L. Peternel, T. Petrič, E. Oztop, J. Babič, Teaching robots to cooperate with humans in dynamic manipulation tasks based on multi-modal human-in-the-loop approach, Autonomous robots 36 (2014) 123–136.

[23] H. Ben Amor, G. Neumann, S. Kamthe, O. Kroemer, J. Peters, Interaction primitives for human-robot cooperation tasks, in: Robotics and Automation (ICRA), 2014 IEEE Intl. Conf. on, pp. 2831–2837.

[24] W. M. Keyserling, D. B. Chaffin, Occupational ergonomics-methods to evaluate physical stress on the job, Annual review of public health 7 (1986) 77–104.

[25] S. E. Mathiassen, T. Möller, M. Forsman, Variability in mechanical exposure within and between individuals performing a highly constrained industrial work task, Ergonomics 46 (2003) 800–824.

[26] S. Kumar, Theories of musculoskeletal injury causation, Ergonomics 44 (2001) 17–47.

[27] G. B. Andersson, Epidemiologic aspects on low-back pain in industry., Spine 6 (1981) 53–60.

[28] S. L. Sauter, L. R. Murphy, J. J. Hurrell, Prevention of work-related psychological disorders: A national strategy proposed by the national institute for occupational safety and health (niosh)., American Psychologist 45 (1990) 1146.

[29] M. Peruzzini, M. Pellicciari, M. Gadaleta, A comparative study on computer-integrated set-ups to design human-centred manufacturing systems, Robotics and Computer-Integrated Manufacturing 55 (2019) 265–278.

[30] M. Millard, T. Uchida, A. Seth, S. L. Delp, Flexing computational muscle: modeling and simulation of musculotendon dynamics, Journal of biomechanical engineering 135 (2013) 021005.

[31] J. Jovic, A. Escande, K. Ayusawa, E. Yoshida, A. Kheddar, G. Venture, Humanoid and human inertia parameter identification using hierarchical optimization, IEEE Transactions on Robotics 32 (2016) 726–735.

[32] S. Gallagher, W. S. Marras, K. G. Davis, K. Kovacs, Effects of posture on dynamic back loading during a cable lifting task, Ergonomics 45 (2002) 380–398.

[33] J. C. E. Van Der Burg, J. H. Van Dieën, H. M. Toussaint, Lifting an unexpectedly heavy object: The effects on low-back loading and balance loss, Clinical Biomechanics 15 (2000) 469–477.

[34] E. A. Sisbot, L. F. Marin-Urias, R. Alami, T. Simeon, A human aware mobile robot motion planner, IEEE Transactions on Robotics 23 (2007) 874–883.

[35] K. Strabala, M. K. Lee, A. Dragan, J. Forlizzi, S. Srinivasa, M. Cakmak, V. Micelli, Towards seamless human-robot handovers, Journal of Human-Robot Interaction 1 (2013).

[36] A. M. Bestick, S. A. Burden, G. Willits, N. Naikal, S. S. Sastry, R. Bajcsy, Personalized kinematics for human-robot collaborative manipulation, in: Intelligent Robots and Systems (IROS), 2015 IEEE/RSJ International Conference on, IEEE, pp. 1037–1044.

[37] B. Navarro, A. Cherubini, A. Fonte, G. Poisson, P. Fraisse, A Framework for intuitive collaboration with a mobile manipulator, in: Intelligent Robots and Systems (IROS), 2015 IEEE/RSJ Intl. Conf. on, pp. 1–8.

[38] N. Vahrenkamp, H. Arnst, M. Wächter, D. Schiebener, P. Sotiropoulos, M. Kowalik, T. Asfour, Workspace analysis for planning human-robot interaction tasks, in: 2016 IEEE-RAS 16th International Conference on Humanoid Robots (Humanoids), pp. 1298–1303.

[39] L. Peternel, C. Fang, N. Tsagarakis, A. Ajoudani, A selective muscle fatigue management approach to ergonomic human-robot co-manipulation, Robotics and Computer-Integrated Manufacturing 58 (2019) 69–79.

[40] W. Kim, J. Lee, N. Tsagarakis, A. Ajoudani, A real-time and reduced-complexity approach to the detection and monitoring of static joint overloading in humans, in: Rehabilitation Robotics (ICORR), 2017 International Conference on, IEEE, pp. 828–834.

[41] W. Kim, J. Lee, L. Peternel, N. Tsagarakis, A. Ajoudani, Anticipatory robot assistance for the prevention of human static joint overloading in human–robot collaboration, IEEE Robotics and Automation Letters 3 (2018) 68–75.

[42] T. Yoshikawa, Manipulability of Robotic Mechanisms, The Intl. Journal of Robotics Research 4 (1985) 3–9.

[43] P. Maurice, P. Schlehuber, V. Padois, Y. Measson, P. Bidaud, Automatic selection of ergonomie indicators for the design of collaborative robots: A virtual-human in the loop approach, in: 2014 IEEE-RAS International Conference on Humanoid Robots, pp. 801–808.

[44] P. Maurice, V. Padois, Y. Measson, P. Bidaud, Experimental assessment of the quality of ergonomic indicators for dynamic systems computed using a digital human model, International Journal of Human Factors Modelling and Simulation 5 (2016) 190–209.

[45] L. Peternel, W. Kim, J. Babič, A. Ajoudani, Towards ergonomic control of human-robot co-manipulation and handover, in: 2017 IEEE-RAS 17th International Conference on Humanoid Robotics (Humanoids), pp. 55–60.

[46] D. A. Winter, Human balance and posture control during standing and walking, Gait & posture 3 (1995) 193–214.

[47] M. B. Popovic, A. Goswami, H. Herr, Ground reference points in legged locomotion: Definitions, biological trajectories and control implications, The International Journal of Robotics Research 24 (2005) 1013–1032.

[48] A. González, M. Hayashibe, V. Bonnet, P. Fraisse, Whole body center of mass estimation with portable sensors: Using the statically equivalent serial chain and a kinect, Sensors 14 (2014) 16955–16971.

[49] P. R. Bélanger, P. Dobrovolny, A. Helmy, X. Zhang, Estimation of angular velocity and acceleration from shaft-encoder mea-

surements, The International Journal of Robotics Research 17 (1998) 1225–1233.

[50] M. Lorenzini, W. Kim, E. De Momi, A. Ajoudani, A synergistic approach to the real-time estimation of the feet ground reaction forces and centers of pressure in humans with application to human–robot collaboration, IEEE Robotics and Automation Letters 3 (2018) 3654–3661.

[51] S. H. Snook, V. M. Ciriello, The design of manual handling tasks: revised tables of maximum acceptable weights and forces, Ergonomics 34 (1991) 1197–1213.

[52] E. Rueckert, J. Čamernik, J. Peters, J. Babič, Probabilistic Movement Models Show that Postural Control Precedes and Predicts Volitional Motor Control., Scientific reports 6 (2016) 28455.

[53] K. Ohta, Y. Tanaka, I. Kawate, T. Tsuji, Human muscular mobility ellipsoid: End-point acceleration manipulability measure in fast motion of human upper arm, Journal of Biomechanical Science and Engineering 9 (2014) 14–00207.

[54] R. Goljat, J. Babič, T. Petrič, L. Peternel, J. Morimoto, Power-augmentation control approach for arm exoskeleton based on human muscular manipulability, in: Robotics and Automation (ICRA), 2017 IEEE Intl. Conf. on, pp. 5929–5934.

[55] S. Hignett, L. McAtamney, Rapid entire body assessment (reba), Applied ergonomics 31 (2000) 201–205.

[56] H. J. Hermens, B. Freriks, R. Merletti, D. Stegeman, J. Blok, G. Rau, C. Disselhorst-Klug, G. Hägg, European Recommendations for Surface Electromyography: Results of the Seniam Project (SENIAM), Enschede, The Netherlands: Roessingh Research and Development, 1999.

[57] C. E. Boettcher, K. A. Ginn, I. Cathers, Standard maximum isometric voluntary contraction tests for normalizing shoulder muscle emg, Journal of orthopaedic research 26 (2008) 1591–1597.

[58] K. Kubo, Y. Kawakami, T. Fukunaga, Influence of elastic properties of tendon structures on jump performance in humans, Journal of applied physiology 87 (1999) 2090–2096.

[59] N. T. Roach, M. Venkadesan, M. J. Rainbow, D. E. Lieberman, Elastic energy storage in the shoulder and the evolution of high-speed throwing in homo, Nature 498 (2013) 483.